Delft University of Technology

Document Version
Final published version

Licence
CC BY

Citation (APA)
Zhang, Y., Kulesh, I., ten Haaf, S. L. D., van Loo, N., Zatelli, F., Degroote, T., Prosko, C. G., & Goswami, S. (2026). Gate Reflectometry in a Minimal Kitaev Chain Device. *PRX Quantum*, *7*(2), Article 020317. https://doi.org/10.1103/7367-wbp9

Important note
To cite this publication, please use the final published version (if applicable).
Please check the document version above.

Copyright
In case the licence states "Dutch Copyright Act (Article 25fa)", this publication was made available Green Open Access via the TU Delft Institutional Repository pursuant to Dutch Copyright Act (Article 25fa, the Taverne amendment). This provision does not affect copyright ownership.
Unless copyright is transferred by contract or statute, it remains with the copyright holder.

Sharing and reuse
Other than for strictly personal use, it is not permitted to download, forward or distribute the text or part of it, without the consent of the author(s) and/or copyright holder(s), unless the work is under an open content license such as Creative Commons.

Takedown policy
Please contact us and provide details if you believe this document breaches copyrights.
We will remove access to the work immediately and investigate your claim.

This work is downloaded from Delft University of Technology.

Gate Reflectometry in a Minimal Kitaev Chain Device

Yining Zhang, Ivan Kulesh, Sebastiaan L.D. ten Haaf, Nick van Loo, Francesco Zatelli, Tijl Degroote, Christian G. Prosko, and Srijit Goswami*
QuTech and Kavli Institute of Nanoscience, Delft University of Technology, Delft 2600 GA, The Netherlands

(Received 18 September 2025; accepted 19 March 2026; published 28 April 2026)

Hybrid quantum dot (QD)-superconductor system can be used to realize Majorana zero modes in artificial Kitaev chains. These chains provide a promising platform for the realization of Majorana qubits. Radio-frequency gate reflectometry is a fast, noninvasive, and sensitive technique that can be used to read out such qubits. In this work, we use gate reflectometry to probe two QDs coupled via a semiconductor-superconductor hybrid segment. We demonstrate that gate sensing can resolve charge stability diagrams and clearly distinguish between elastic cotunneling and crossed-Andreev reflection, the two key processes that allow one to form a Kitaev chain. Furthermore, we show that this information is accessible, even when the system is completely decoupled from the normal leads. In this closed regime, we show that the observed quantum-capacitance signal is indicative of parity switching between the even and odd ground states. Our measurements in both open and closed regimes confirm that gate reflectometry captures the essential features of interdot coupling and parity dynamics.

DOI: 10.1103/7367-wbp9

I. INTRODUCTION

Hybrid systems with quantum dots (QDs) coupled to superconductors [1–3] allow for engineering Majorana zero modes in artificial Kitaev chains [4]. With the recent realization of minimal Kitaev chains [5,6] there now exist concrete proposals to use such systems to implement Majorana-based qubits [2,7,8] and to demonstrate non-Abelian operations [8–10]. In order to read out such qubits, fast measurement techniques are crucial. Radio-frequency (RF) reflectometry has been demonstrated as a powerful readout technique, enabling high-speed, noninvasive detection of quantum dot charge and spin states by monitoring impedance changes in resonator circuits [11,12]. RF sensing has been widely used to sense charge [13–17] and spin [18–20] in QD arrays. More recently, RF reflectometry has been applied to QD-superconductor hybrid systems to sense Cooper pair splitting [21,22] and quasiparticle poisoning (QPP) [23–26]. Gate-based RF reflectometry is particularly well suited for probing Kitaev chains, as it integrates naturally with quantum dots—the essential building blocks of these hybrid systems—enabling compact, noninvasive access to probe the system.

In this work, we use gate reflectometry techniques to study a minimal Kitaev chain device in a two-dimensional electron gas (2DEG) with two quantum dots coupled by a semiconductor-superconductor hybrid segment. We perform experiments in two measurement configurations: with or without normal reservoirs. When the system is coupled to normal leads, we can measure charge stability diagrams (CSDs) with both lead reflectometry and gate reflectometry. Gate reflectometry can clearly distinguish the type of coupling between QDs, consistent with lead reflectometry measurements. When the system is decoupled from the normal leads, gate reflectometry can still be used to probe the quantum capacitance of the system, and we observed quantum capacitance from even and odd ground state transitions. The observation of both even and odd parity in the same measurement indicates that the ground state of the system can switch by quasiparticle poisoning. We verify this by partially coupling the normal leads, allowing us to artificially inject quasiparticles into the system.

II. METHODS

Figure 1(a) shows a false-color scanning electron microscopic image of a device that is lithographically identical to the one measured. The device is fabricated on an InSbAs-Al 2DEG [27]. There are three layers of gates: the first layer (red) defines the one-dimensional channel; the second layer (blue) independently controls the chemical potential of each section; and the third layer (pink) defines the tunnel barriers. Each gate layer is separated by 20 nm

*Contact author: s.goswami@tudelft.nl

Published by the American Physical Society under the terms of the Creative Commons Attribution 4.0 International license. Further distribution of this work must maintain attribution to the author(s) and the published article's title, journal citation, and DOI.

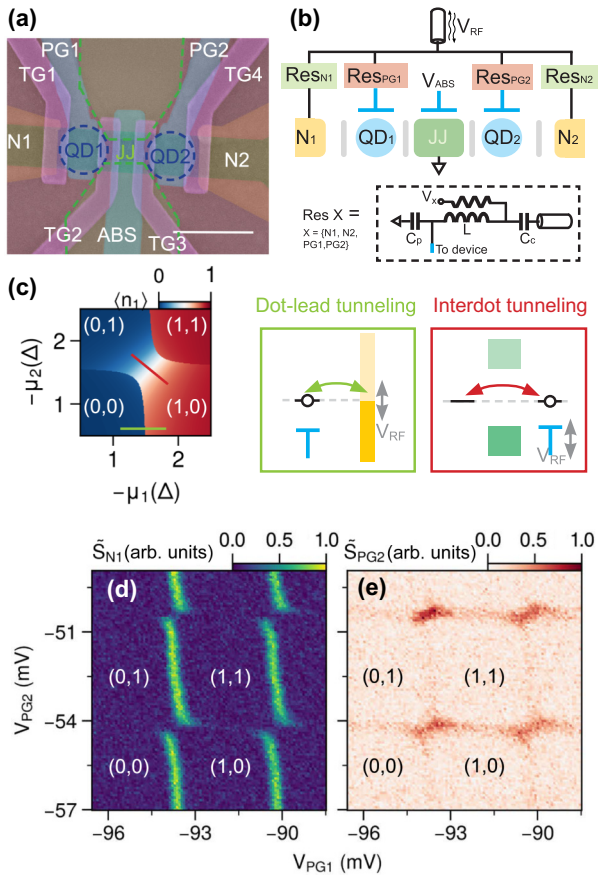

FIG. 1. Experimental setup and charge stability diagrams. (a) False-color SEM image of the device with labeled electrostatic gates and metallic leads. The two Al leads outlined with dashed green lines in Fig. 1(a) are connected by a loop [see Fig. S1(a) in the Supplemental Material [28]]. The scale bar represents 500 nm. (b) Schematic of the RF circuit. The bottom panel shows a schematic of each resonator, consisting of a parasitic capacitance C_p, an inductor L, a coupling capacitor C_c, and a resistor as the bias tee. (c) Left: simulated charge occupation number on QD1. Sharp contours separate ground states with different parity (e.g., the green mark), while within a single parity sector, the charge occupation changes smoothly (e.g., the red mark). Middle and right: schematic energy diagrams for the tunneling processes corresponding to the two markers. (d) and (e) Charge stability diagrams measured from normal lead N1 and on plunger gate PG2, respectively.

dielectric Al_2O_3. The two QDs are coupled by a Josephson junction (JJ) that hosts Andreev bound states (ABSs). The junction is formed by two aluminum tips (colored green with dashed outline). The full device SEM image and basic characterization of the QDs and JJ can be found in Fig. S1 in the Supplemental Material [28].

A resonator chip is used to perform multiplexed RF sensing [29]. The schematic of the RF circuit is shown in Fig. 1(b). There are four resonators used in this experiment: two of them connect to the two normal leads, and two of them connect to the two QD plunger gates. The lower panel of Fig. 1(b) shows a schematic of an individual resonator with a bias tee that allows the application of DC bias or gate voltage to the device. The reflected complex voltage S_{11} is recorded for each resonator. For better visualization, the signal is projected onto a line that maximizes the signal magnitude and normalized to a single real value $\tilde{S}$. The detailed signal analysis method is described in Fig. S4 in the Supplemental Material [28].

When resonant tunneling occurs between normal leads and the device or between the two QDs, the impedance of the device changes. The impedance change results in changes in S_{11}. More specifically, the resistive component of the device changes the magnitude of the resonator response, while the capacitive component shifts the resonator frequency [12]. In low-dimensional quantum systems, like QDs, charge tunneling causes a small correction term of the total capacitance of the gate electrode due to the finite density of states in the system [12,30,31]. This is known as quantum capacitance, given by $C_q = e^2 \frac{dN}{d\mu}$, where N is the charge expectation and μ is the chemical potential. Notably, the main contribution to our signal—quantum capacitance—arises only when charge states are coherently hybridized [11,32].

To understand the quantum-capacitance signal of a DQD system better, a calculation of the charge expectation number of a QD in a double quantum dot (DQD) system is shown in Fig. 1(c) on the left. At the bottom left corner and the top right corner, the ground state parity of DQD is even, i.e., $(0,0)$ or $(1,1)$. A sharp contour distinguishes the even and odd ground states. At the charge degeneracy points where two charge states $(0,1)$ and $(1,0)$ start to hybridize [red marker in Fig. 1(c), left panel], electrons can hop between the two QD levels [shown schematically in Fig. 1(c), right panel]. This interdot hopping results in a change in quantum capacitance (since it is proportional to $d\langle N_1 \rangle / d\mu_1$) and is detectable in the gate-sensing signal. On the other hand, when the charge occupation number of the ground state changes, as indicated by the green marker, electrons can tunnel from the normal lead to the DQD, thereby switching the parity of DQD [schematic in the middle panel of Fig. 1(c)]. This process will result in a strong response on the lead resonator.

III. RESULTS

A. Using gate sensing to probe the interdot coupling

It has been well established that transport measurements of CSDs can reveal the type of coupling between QDs [33–35]. To verify that gate sensing provides the same information, we simultaneously measure a CSD with gate reflectometry on PG2 [Fig. 1(d)] and lead reflectometry via N1 [Fig. 1(e)]. The tunnel barrier between QD2 and the normal lead (TG4) is pinched off, while the outer barrier for QD1 (TG1) is configured to the tunneling regime.

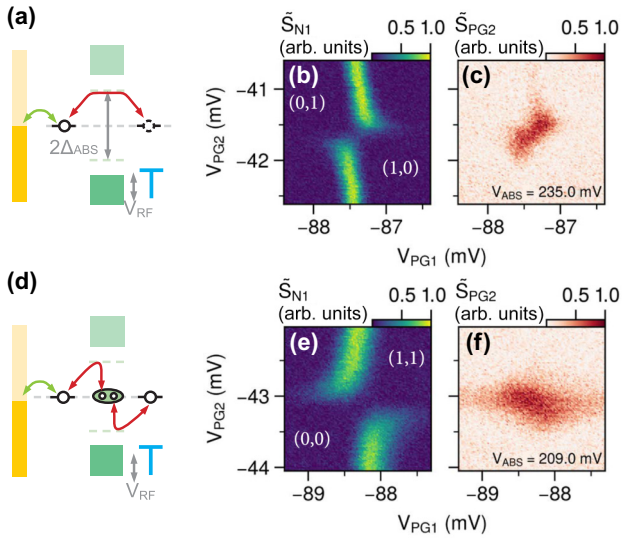

FIG. 2. Gate sensing of the interdot couplings. (a) Schematic of elastic cotunneling coupling. The green dashed lines represent the Andreev bound state energy levels. The red arrow indicates the interdot hopping mediated by the Andreev bound state. (b) and (c) Charge stability diagrams with normalized reflected radio-frequency voltage $\tilde{S}$ on N1 (b) and PG2 (c) in the elastic cotunneling-dominated regime. (d) Schematic of cross Andreev reflection coupling. (e) and (f) Charge stability diagram with normalized reflected radio-frequency voltage $\tilde{S}$ on N1 (e) and PG2 (f) in the cross Andreev reflection-dominated regime. The coupling type can be tuned by sweeping the Andreev bound state gate voltage V_{ABS}.

Sweeping the plunger gates of the two QDs, we can measure tunneling processes in different sections of the device. When a dot level aligns with the Fermi level, dot-lead tunneling occurs, which results in a strong signal on the lead resonator. This process corresponds to the signal shown in Fig. 1(d). Near joint charge degeneracy points, the two charge states in the two QDs start to hybridize, indicated by the avoided crossings in the CSDs. The resonator response only shows QD1 Coulomb resonances because QD2 is decoupled from the normal lead N2 by pinching off TG4 barrier. When we use gate sensing to read out the same CSD, the resonator instead responds strongly when the system reaches a joint charge degeneracy point. As discussed earlier, a quantum-capacitance signal appears when charge distribution changes adiabatically. We observe the resonator response exactly at the avoided crossings in Fig. 1(d), indicating interdot tunneling. When the dot levels are far away from the degeneracy point or in Coulomb blockade, the tunneling is suppressed and gate sensing gives no response. Therefore, we confirm that gate sensing provides complementary information about the system, consistent with RF reflectometry measurements from the normal lead.

Having shown that our setup is capable of measuring CSDs with gate sensing, we proceed with probing different kinds of couplings between the two QDs. The presence of the superconductor and ABSs allows for tunable elastic cotunneling (ECT) and cross Andreev reflection (CAR) between the QDs [33,34,36], which is instrumental for the realization of artificial Kitaev chains [5,6]. Detecting the dominant type of coupling is important for tuning up these Kitaev chains. The type of interdot coupling can be controlled by changing the chemical potential of the hybrid region. ECT occurs when coherent hybridization between the dot levels in the odd parity manifold; an electron can tunnel from one dot to the other mediated by the ABS. In the CSD measured by lead reflectometry, an antidiagonal avoided crossing is shown in Fig. 2(b) with the $(0,1)$ and $(1,0)$ region connected, which is the signature of the ECT coupled regime. The same measurement with gate reflectometry has a strong signal in the diagonal direction in Fig. 2(c), corresponding to the interdot tunneling near the charge degeneracy point. By sweeping the V_{ABS} gate voltage, we can tune the interdot coupling from ECT-like to CAR-like. A schematic of the CAR process is shown in Fig. 2(d). When the CAR coupling is dominant and two quantum dot levels are antisymmetric along the Fermi level, two electrons can form or split a Cooper pair mediated by Andreev bound states [33,34,36]. In the CSD shown in Fig. 2(e), the direction of the avoided crossing changed from antidiagonal to diagonal, connecting the $(0,0)$ and $(1,1)$ in the CSD. Near the charge degeneracy point, a strong gate-sensing signal arises along the antidiagonal direction. Therefore, from the direction of the gate-sensing signal we can infer the type of coupling between the two QDs. We also show in Fig. S8 in the Supplemental Material [28] how the gate-sensing signal evolves as V_{ABS} is tuned through the Majorana sweet spot condition, where the amplitudes of ECT and CAR are equal.

B. Gate sensing in a closed double dot system

A minimal Majorana parity qubit device comprises of two pairs of the DQD, and their joint parity (either even or odd) can be used as the basis of the qubit [2]. When implementing a parity qubit, it is necessary to decouple the system from the leads to prevent relaxation and quasiparticle poisoning. In this configuration, while lead reflectometry is no longer available, gate sensing can still be used to probe the system. To demonstrate this, we pinch off both tunnel barriers (TG1 and TG4) to decouple the system from normal reservoirs and study the system via gate sensing.

The alternating RF voltages on the plunger gates (PG1 and PG2) allow for electron tunneling between the two dots or between a QD and the ABS, resulting in the quantum-capacitance signals. We find that the CSDs of a closed system measured by gate sensing [Figs. 3(a) and 3(b)] look significantly different to the open system

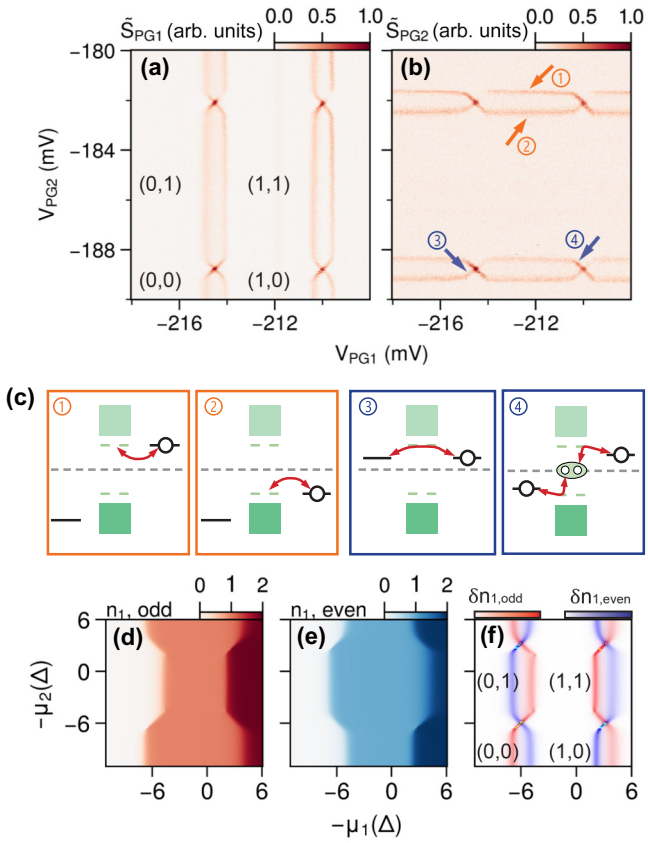

FIG. 3. Gate reflectometry charge stability diagrams of a closed system. (a) and (b) Charge stability diagrams measured by gate reflectometry on the plunger gates of both quantum dots. Blue and orange arrows indicate different tunneling processes, as illustrated in (c). (c) Schematics of the possible tunneling processes labeled in (b). Processes ① and ② correspond to quantum dot-Andreev bound state tunneling when one dot is off resonance and the other dot level aligned with the Andreev bound state energy. Processes ③ and ④ correspond to the interdot tunneling events when both dot levels are below the Andreev bound state energy (elastic cotunneling and cross Andreev reflection). (d) and (e) Numerical simulation of charge expectation number for the odd and even ground states of one dot in a DQD coupled by Andreev bound state. (f) Numerical derivative of the ground state charge with respect to the chemical potential of QD1, μ_1. The signal qualitatively represents quantum capacitance (C_q) measured via gate reflectometry. The plot has contributions of C_q from both the odd and even ground states.

[Fig. 1(e)]. We observe Coulomb blockade (white background) separated by dot resonance signals. The relative charge occupation is labeled in Fig. 3(a). Instead of one strong Coulomb peak when the QD is on resonance [as shown in Fig. 1(d)], we observe two parallel lines, as indicated by the orange arrows in Fig. 3(b). Near the joint charge degeneracy points, we observed crosslike signals, indicated by the blue arrows in Fig. 3(b).

In order to understand the microscopic origin of these features we schematically outline the relevant tunneling processes [Fig. 3(c)]. When a QD level is aligned with the ABS level and the other dot is off resonance, electrons can hop between the QD and the ABS, as illustrated in Fig. 3(c) ① and ②. Similar tunneling process can also occur directly between the two QDs when they are aligned or antialigned within the ABS level. In these cases, the QDs hybridize due to ECT [Fig. 3(c) ③] or CAR [Fig. 3(c) ④] coupling mediated by the ABS. The corresponding features present themselves near the joint charge degeneracy points, shown as a crosslike pattern. We note that a dominant coupling mechanism is not immediately obvious, based just on these crossing features. However, we find the crossings change qualitatively while we sweep the ABS gate voltage, as shown in Fig. S6 in the Supplemental Material [28].

To get a better understanding of the double line feature, we compare our experiments with a simple numerical simulation of the quantum capacitance for a DQD coupled by ABS [3,35] (detailed description in the Supplemental Material [28]). We begin with considering the even and odd ground states separately and calculate the charge occupation of each QD in odd and even ground states as the function of chemical potential of the two dots. The charge occupation of QD1 at odd and even ground states is plotted in Figs. 3(d) and 3(e), respectively. As we sweep the chemical potential of QD1, the occupation changes from 0 to 2 with distinct steps. The qualitative representation of quantum-capacitance signal can be determined by taking derivative of $\langle N \rangle$. The derivative of charge of odd state and even state is plotted in Fig. 3(f) with red and blue, respectively.

If the DQD is coupled to normal leads, the system can always relax to the lowest energy ground state by exchanging electrons with the reservoirs in order to flip the parity when necessary. However, when the DQD is decoupled from normal reservoirs, ideally the system maintains a fixed parity, because no electrons can tunnel from the normal lead. If this were the case, we should have observed the signal corresponding to only one parity state. Instead, we observe the quantum-capacitance signal corresponding to both even and odd states, which indicates parity flipping within the integration time of each data point. We attribute this parity flipping mechanism to QPP which is one of the potential decoherence sources for Majorana-based qubits [37,38]. The source of this QPP could either be the superconducting leads where Cooper pairs are broken by some high-energy processes, or from the normal leads, due to a residual coupling to the DQD. In Fig. S7 in the Supplemental Material [28] we present CSDs at different TG4 values (thus different couplings to the normal lead). The double line feature emerges as TG4 goes more negative (weaker coupling to N2), supporting our interpretation that this feature originates from QPP, and is visible when relaxation to the normal lead is suppressed.

C. Poisoning from the normal reservoir

In order to study the effect of the normal leads on the poisoning, we slightly reduce the barrier to N2 (by modifying TG4), while ensuring that the measured current remains below the noise floor of our current meter. When the bias voltage is kept at 0, the CSD remains similar to the case where the normal lead is fully decoupled, as shown in Fig. 4(b). In this case, quantum-capacitance signals from both even and odd states show comparable strength. By applying a bias voltage to N2, we artificially induce poisoning in the system. We measure the CSD with $-200\ \mu$V bias voltage applied on N2, shown in Fig. 4(a). Compared to Fig. 4(b), the lower branch of the quantum-capacitance signal is significantly enhanced, as indicated by the blue arrow. The schematic energy diagram in Fig. 4(d) illustrates the mechanism: when the bias is below the Fermi level and lower than the ABS energy, holes preferentially tunnel into the system, increasing the occupation of the lower ABS branch and thereby showing a stronger signal in the CSD. Similarly, when a $+200\ \mu$V bias is applied to N2, the upper branch of the signal becomes more pronounced, as shown in Fig. 4(c) and highlighted by the orange arrow. The corresponding schematic in Fig. 4(e) shows that, in this case, electrons more readily tunnel into the state above the Fermi level, enhancing the population of the upper ABS branch and its gate reflectometry signal.

A finer bias dependence measurement with only QD2 on resonance is shown in Fig. 4(f). Here we measure the gate sensor response as a function of the plunger gate voltage of QD2 V_{PG2} and bias voltage V_2. The two lines indicate when the QD level aligns with the ABS. Along the left resonance, the signal strength rises significantly below $-125\ \mu$V, which can be interpreted as the point where Fermi level in N2 aligns with the QD2 and ABS energy levels. Along the right resonance, the signal is stronger above $+125\ \mu$V. The signal strengths are plotted in the right panel in Fig. 4(f). Combining the two linecuts together allows us to extract the ABS energy gap $2\Delta_{ABS} \approx 250\,\mu$V The ABS energy can also be independently extracted from the CSDs by converting V_{PG2} to an energy, through the PG2 lever arm. Given the lever arm of PG2 is 0.31 (see the Supplemental Material [28]), and the voltage difference between the double lines is 0.82 mV, we estimate $2\Delta_{ABS} = 254.2\ \mu$V, which agrees well with the gap size extracted from Fig. 4(f), thus supporting our interpretation for the origin of the gate-sensing signal.

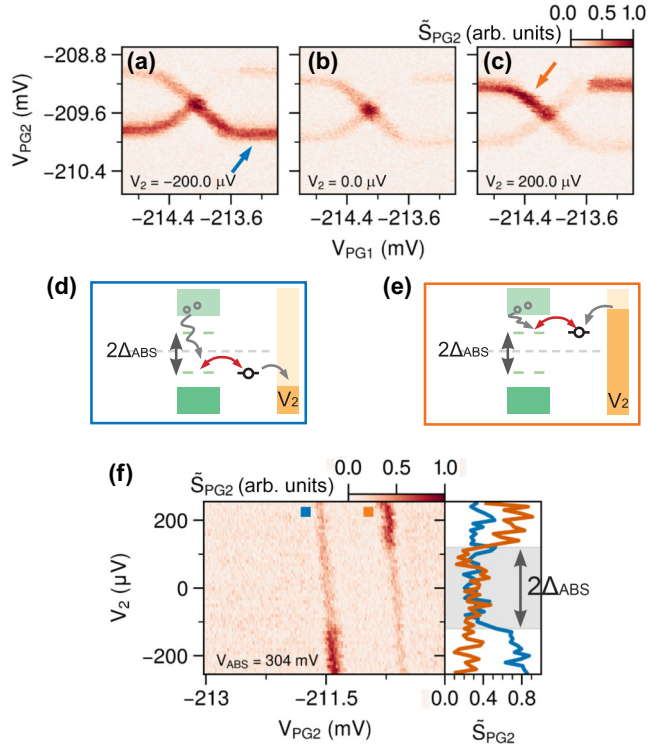

FIG. 4. Effect of the normal lead. (a)–(c) Charge stability diagrams measured by gate reflectometry on QD2 under different bias voltages V_2 (annotated in each panel). The arrows in (a) and (c) indicate the enhanced tunneling processes. (d) and (e) Schematic energy diagrams illustrating possible poisoning events originating from the superconductor and the normal lead, corresponding to the arrows in (a) and (c), respectively. (f) Gate reflectometry signal on QD2 as a function of V_2, with QD1 off resonance. The right panel shows the amplitude of $\tilde{S}_{PG2}$ along the dashed line in the main plot. The weaker portion of the signal corresponds to the Andreev bound state energy gap.

IV. CONCLUSIONS

In this work, we have shown that gate sensing can be used to probe a Kitaev chain device where two QDs are coupled via tunable ABSs. In an open system, coupled to the normal leads, we demonstrated that gate reflectometry allows us to distinguish between ECT and CAR mediated coupling between the QDs. In a closed system the gate-sensing signal reflects the quantum capacitance of the system and provides information about the ground state parity. In particular we find that quasiparticle poisoning events lead to fast switching of the ground state parity. Furthermore, we identified the normal reservoirs as a potential source of poisoning, confirmed by artificially injecting quasiparticles into the QD. In order to use gate reflectometry to study Kitaev chain-based parity qubits in the future, it is important to understand in more detail the mechanisms that limit the parity lifetime in our devices and to develop protocols to use the gate-sensing signal to tune up Kitaev devices in the absence of normal leads. Furthermore, it is also important to consider that quantum-capacitance measurements alone may not reliably provide information about the Majorana polarization, an important metric for the qubit quality [8]. Addressing this challenge will likely require complementary probes and/or measurements sensitive to the Majorana polarization.

ACKNOWLEDGMENTS

We thank Di Xiao, Candice Thomas, and Michael J. Manfra for providing the semiconductor heterostructures used in this work. We thank O. W. B. Benningshof and J. D. Mensingh for technical assistance with the cryogenic electronics. The research at Delft was supported by the Dutch National Science Foundation (NWO), Microsoft Corporation Station Q, and a grant from Top consortium for Knowledge and Innovation program (TKI). S.G. acknowledges financial support from the Horizon Europe Framework Program of the European Commission through the European Innovation Council Pathfinder Grant No. 101115315 (QuKiT).

I.K. fabricated the device, with input from C.G.P. Y.Z. and I.K. fabricated the resonator circuits. C.G.P. and I.K. designed the measurement setup. Measurements were performed by Y.Z., I.K., S.L.D.t.H., and T.D. N.v.L. and F.Z. contributed to understanding and interpretation of the data through regular discussions. The manuscript was written by Y.Z. and S.G., with input from all coauthors. S.G. supervised the experimental work in Delft.

DATA AVAILABILITY

The data that support the findings of this article are openly available [39].

[1] J. D. Sau and S. D. Sarma, Realizing a robust practical Majorana chain in a quantum-dot-superconductor linear array, Nat. Commun. **3**, 964 (2012).

[2] M. Leijnse and K. Flensberg, Parity qubits and poor man's Majorana bound states in double quantum dots, Phys. Rev. B: Condens. Matter Mater. Phys. **86**, 134528 (2012).

[3] A. Tsintzis, R. S. Souto, and M. Leijnse, Creating and detecting poor man's Majorana bound states in interacting quantum dots, Phys. Rev. B **106**, L201404 (2022).

[4] A. Y. Kitaev, Unpaired Majorana fermions in quantum wires, Phys.-Usp. **44**, 131 (2001).

[5] T. Dvir, G. Wang, N. van Loo, C.-X. Liu, G. P. Mazur, A. Bordin, S. L. D. ten Haaf, J.-Y. Wang, D. van Driel, F. Zatelli *et al.*, Realization of a minimal Kitaev chain in coupled quantum dots, Nature **614**, 445 (2023).

[6] S. L. D. ten Haaf, Q. Wang, A. M. Bozkurt, C.-X. Liu, I. Kulesh, P. Kim, D. Xiao, C. Thomas, M. J. Manfra, T. Dvir *et al.*, A two-site Kitaev chain in a two-dimensional electron gas, Nature **630**, 329 (2024).

[7] G. Széchenyi and A. Pályi, Parity-to-charge conversion for readout of topological Majorana qubits, Phys. Rev. B **101**, 235441 (2020).

[8] A. Tsintzis, R. S. Souto, K. Flensberg, J. Danon, and M. Leijnse, Majorana qubits and non-Abelian physics in quantum dot–based minimal Kitaev chains, PRX Quantum **5**, 010323 (2024).

[9] C.-X. Liu, H. Pan, F. Setiawan, M. Wimmer, and J. D. Sau, Fusion protocol for Majorana modes in coupled quantum dots, Phys. Rev. B **108**, 085437 (2023).

[10] P. Boross and A. Pályi, Braiding-based quantum control of a Majorana qubit built from quantum dots, Phys. Rev. B **109**, 125410 (2024).

[11] M. Esterli, R. Otxoa, and M. Gonzalez-Zalba, Small-signal equivalent circuit for double quantum dots at low-frequencies, Appl. Phys. Lett. **114**, 253505 (2019).

[12] F. Vigneau, F. Fedele, A. Chatterjee, D. Reilly, F. Kuemmeth, M. F. Gonzalez-Zalba, E. Laird, and N. Ares, Probing quantum devices with radio-frequency reflectometry, Appl. Phys. Rev. **10**, 021305 (2023).

[13] M. Urdampilleta, A. Chatterjee, C. C. Lo, T. Kobayashi, J. Mansir, S. Barraud, A. C. Betz, S. Rogge, M. F. Gonzalez-Zalba, and J. J. Morton, Charge dynamics and spin blockade in a hybrid double quantum dot in silicon, Phys. Rev. X **5**, 031024 (2015).

[14] D. De Jong, J. Van Veen, L. Binci, A. Singh, P. Krogstrup, L. P. Kouwenhoven, W. Pfaff, and J. D. Watson, Rapid detection of coherent tunneling in an in as nanowire quantum dot through dispersive gate sensing, Phys. Rev. Appl. **11**, 044061 (2019).

[15] D. Reilly, C. Marcus, M. Hanson, and A. Gossard, Fast single-charge sensing with a RF quantum point contact, Appl. Phys. Lett. **91**, 162101 (2007).

[16] C. Barthel, M. Kjærgaard, J. Medford, M. Stopa, C. M. Marcus, M. Hanson, and A. C. Gossard, Fast sensing of double-dot charge arrangement and spin state with a radio-frequency sensor quantum dot, Phys. Rev. B: Condens. Matter Mater. Phys. **81**, 161308 (2010).

[17] C. Prosko, I. Kulesh, M. Chan, L. Han, D. Xiao, C. Thomas, M. Manfra, S. Goswami, and F. K. Malinowski, Flux-tunable hybridization in a double quantum dot interferometer, SciPost Phys. **17**, 074 (2024).

[18] F. Fedele, A. Chatterjee, S. Fallahi, G. C. Gardner, M. J. Manfra, and F. Kuemmeth, Simultaneous operations in a two-dimensional array of singlet-triplet qubits, PRX Quantum **2**, 040306 (2021).

[19] A. West, B. Hensen, A. Jouan, T. Tanttu, C.-H. Yang, A. Rossi, M. F. Gonzalez-Zalba, F. Hudson, A. Morello, D. J. Reilly *et al.*, Gate-based single-shot readout of spins in silicon, Nat. Nanotechnol. **14**, 437 (2019).

[20] A. Betz, R. Wacquez, M. Vinet, X. Jehl, A. Saraiva, M. Sanquer, A. Ferguson, and M. Gonzalez-Zalba, Dispersively detected Pauli spin-blockade in a silicon nanowire field-effect transistor, Nano Lett. **15**, 4622 (2015).

[21] D. de Jong, C. G. Prosko, L. Han, F. K. Malinowski, Y. Liu, L. P. Kouwenhoven, and W. Pfaff, Controllable single cooper pair splitting in hybrid quantum dot systems, Phys. Rev. Lett. **131**, 157001 (2023).

[22] J. Van Veen, D. De Jong, L. Han, C. Prosko, P. Krogstrup, J. D. Watson, L. P. Kouwenhoven, and W. Pfaff, Revealing charge-tunneling processes between a quantum dot and a superconducting island through gate sensing, Phys. Rev. B **100**, 174508 (2019).

[23] G. C. Ménard, F. K. Malinowski, D. Puglia, D. I. Pikulin, T. Karzig, B. Bauer, P. Krogstrup, and C. M. Marcus, Suppressing quasiparticle poisoning with a voltage-controlled filter, Phys. Rev. B **100**, 165307 (2019).

[24] H. Nguyen, D. Sabonis, D. Razmadze, E. Mannila, V. Maisi, D. van Zanten, E. O'Farrell, P. Krogstrup, F. Kuemmeth, J. Pekola *et al.*, Electrostatic control

of quasiparticle poisoning in a hybrid semiconductor-superconductor island, Phys. Rev. B **108**, L041302 (2023).

[25] M. A. Quantum, M. Aghaee, A. A. Ramirez, Z. Alam, R. Ali, M. Andrzejczuk, A. Antipov, M. Astafev, A. Barzegar, B. Bauer *et al.*, Interferometric single-shot parity measurement in InAs–Al hybrid devices, Nature **638**, 651 (2025).

[26] N. van Loo, F. Zatelli, G. O. Steffensen, B. Roovers, G. Wang, T. Van Caekenberghe, A. Bordin, D. van Driel, Y. Zhang, W. D. Huisman *et al.*, Single-shot parity readout of a minimal Kitaev chain, Nature **650**, 334 (2026).

[27] C. M. Moehle, C. T. Ke, Q. Wang, C. Thomas, D. Xiao, S. Karwal, M. Lodari, V. van de Kerkhof, R. Termaat, G. C. Gardner *et al.*, InSbAs two-dimensional electron gases as a platform for topological superconductivity, Nano Lett. **21**, 9990 (2021).

[28] See Supplemental Material at http://link.aps.org/supplemental/10.1103/7367-wbp9, which includes Refs. [17,35, 40–43].

[29] J. Hornibrook, J. Colless, A. Mahoney, X. Croot, S. Blanvillain, H. Lu, A. Gossard, and D. Reilly, Frequency multiplexing for readout of spin qubits, Appl. Phys. Lett. **104**, 103108 (2014).

[30] R. Ashoori, H. Stormer, J. Weiner, L. Pfeiffer, S. Pearton, K. Baldwin, and K. West, Single-electron capacitance spectroscopy of discrete quantum levels, Phys. Rev. Lett. **68**, 3088 (1992).

[31] K. Petersson, C. Smith, D. Anderson, P. Atkinson, G. Jones, and D. Ritchie, Charge and spin state readout of a double quantum dot coupled to a resonator, Nano Lett. **10**, 2789 (2010).

[32] R. Mizuta, R. Otxoa, A. Betz, and M. F. Gonzalez-Zalba, Quantum and tunneling capacitance in charge and spin qubits, Phys. Rev. B **95**, 045414 (2017).

[33] G. Wang, T. Dvir, G. P. Mazur, C.-X. Liu, N. van Loo, S. L. D. ten Haaf, A. Bordin, S. Gazibegovic, G. Badawy, E. P. Bakkers *et al.*, Singlet and triplet cooper pair splitting in hybrid superconducting nanowires, Nature **612**, 448 (2022).

[34] Q. Wang, S. L. D. ten Haaf, I. Kulesh, D. Xiao, C. Thomas, M. J. Manfra, and S. Goswami, Triplet correlations in Cooper pair splitters realized in a two-dimensional electron gas, Nat. Commun. **14**, 4876 (2023).

[35] F. Zatelli, D. van Driel, D. Xu, G. Wang, C.-X. Liu, A. Bordin, B. Roovers, G. P. Mazur, N. van Loo, J. C. Wolff *et al.*, Robust poor man's Majorana zero modes using Yu-Shiba-Rusinov states, Nat. Commun. **15**, 7933 (2024).

[36] C.-X. Liu, G. Wang, T. Dvir, and M. Wimmer, Tunable superconducting coupling of quantum dots via Andreev bound states in semiconductor-superconductor nanowires, Phys. Rev. Lett. **129**, 267701 (2022).

[37] G. Goldstein and C. Chamon, Decay rates for topological memories encoded with Majorana fermions, Phys. Rev. B: Condens. Matter Mater. Phys. **84**, 205109 (2011).

[38] J. C. Budich, S. Walter, and B. Trauzettel, Failure of protection of Majorana based qubits against decoherence, Phys. Rev. B **85**, 121405 (2012).

[39] Y. Zhang, Data and code for "probing a minimal Kitaev chain with gate reflectometry" (2025), https://zenodo.org/records/15848623.

[40] I. Kulesh, S. L. D. ten Haaf, Q. Wang, V. P. M. Sietses, Y. Zhang, S. R. Roelofs, C. G. Prosko, D. Xiao, C. Thomas, M. J. Manfra, and S. Goswami, Flux-controlled two-site Kitaev chain, Phys. Rev. Lett. **135**, 056301 (2025).

[41] S. Probst, F. Song, P. A. Bushev, A. V. Ustinov, and M. Weides, Efficient and robust analysis of complex scattering data under noise in microwave resonators, Rev. Sci. Instrum. **86**, 024706 (2015).

[42] M. S. Khalil, M. Stoutimore, F. Wellstood, and K. Osborn, An analysis method for asymmetric resonator transmission applied to superconducting devices, J. Appl. Phys. **111**, 054510 (2012).

[43] F. K. Malinowski, L. Han, D. De Jong, J.-Y. Wang, C. G. Prosko, G. Badawy, S. Gazibegovic, Y. Liu, P. Krogstrup, E. P. Bakkers *et al.*, Radio-frequency *C-V* measurements with subattofarad sensitivity, Phys. Rev. Appl. **18**, 024032 (2022).